High-Pressure Structural Systematics in Neodymium to 302 GPa

High-Pressure Structural Systematics in Neodymium to 302 GPa

S. E. Finnegan, C. V. Storm, E. J. Pace, and M. I. McMahon
SUPA, School of Physics and Astronomy, and Centre for Science at Extreme Conditions, The University of Edinburgh, Peter Guthrie Tait Road, Edinburgh EH9 3FD, United Kingdom

S. G. MacLeod
AWE, Aldermaston, Reading RG7 4PR, United Kingdom and SUPA, School of Physics and Astronomy, and Centre for Science at Extreme Conditions, The University of Edinburgh, Peter Guthrie Tait Road, Edinburgh EH9 3FD, United Kingdom

E. Plekhanov, N. Bonini, and C. Weber
Theory and Simulation of Condensed Matter (TSCM), Department of Physics, Kings College London, The Strand, London WC2R 2LS, United Kingdom

(Dated: April 13, 2021)

Angle-dispersive x-ray powder diffraction experiments have been performed on neodymium metal to a pressure of 302 GPa. Up to 70 GPa we observe the $hP4 \rightarrow cF4 \rightarrow hR24 \rightarrow oI16 \rightarrow hP3$ transition sequence reported previously. At 71(2) GPa we find a transition to a phase which has an orthorhombic structure ($oF8$) with 8 atoms in the unit cell, space group $Fddd$. This structure is the same as that recently observed in samarium above 93 GPa, and is isostructural with high-pressure structures found in the actinides Am, Cf and Cm. We see a further phase transition at 98(1) GPa to a phase with the orthorhombic α-U ($oC4$) structure, which remains stable up to 302 GPa, the highest pressure reached in this study. Electronic structure calculations find the same structural sequence, with calculated transition pressures of 66 and 88 GPa, respectively, for the $hP3 \rightarrow F8$ and $oF8 \rightarrow C4$ transitions. The calculations further predict that $oC4$-Nd loses its magnetism at 100 GPa, in agreement with previous experimental results, and it is the accompanying decrease in enthalpy and volume that results in the transition to this phase. Comparison calculations on the $oF8$ and $oC4$ phases of Sm show that they both retain their magnetism to at least 240 GPa, with the result that $oC4$-Sm is calculated to have the lowest enthalpy over a narrow pressure region near 200 GPa at 0 K.

I. INTRODUCTION

The predominantly trivalent lanthanide metals (La to Lu, excluding Ce, Eu, and Yb) exhibit a common series of structural phase transformations with increasing pressure: hcp ($hP2$ in Pearson notation) $\rightarrow$ Sm-type ($hR9$) $\rightarrow$ dhcp ($hP4$) $\rightarrow$ fcc ($cF4$) $\rightarrow$ distorted-fcc ($hR24$, $oI16$, or $oS8$)[1–4]. This transition sequence is thought to arise from increases in occupation of the $5d$ states as a result of pressure-induced s- to d-electron transfer[5]. Under further compression, the distorted-fcc phases undergo first-order volume collapse transitions into more complex phases, the low-symmetry structures of which are reported to be a result of the participation of $4f$ electrons in the bonding[6], although this has been questioned in more recent publications[7–10].

In Nd and Sm, the structure of the initial phase seen after the volume collapse is reported to be hexagonal with spacegroup $P6_222$ and 3 atoms per unit cell ($hP3$), a structure otherwise seen only in Yb[11]. On further compression, both Nd and Sm are then reported[12] to transform into a monoclinic structure (spacegroup $C2/m$, $mC4$) first observed in Ce at high pressure over 40 years ago[13], and subsequently reported in Gd, Tb, Dy, Ho, Er and Tm[14–19].

However, we have recently shown[20,21] that the $mC4$ structure does not account for all of the observed peaks in the diffraction profiles from Gd-Tm, and that a better fit can be obtained with a 16-atom orthorhombic structure, space group $Fddd$ ($oF16$), that is isosymmetric with the $oF8$ structure seen in the actinides Cf, Am and Cm at high pressure. A comparison of the published diffraction pattern from Nd at 89 GPa[22] with those from the $oF8$ phases of Cf, Am and Cm[23–25] revealed them to be very similar, suggesting that the post-$hP3$ phase of Nd has the $oF8$ structure rather than the $oF16$ structure seen in the higher-Z lanthanides. A subsequent diffraction study of Sm to 222 GPa revealed than the post-$hP3$ phase of Sm also has the $oF8$ structure at pressures above 93 GPa[21].

Unlike in Sm, however, the $oF8$ phase of Nd is known to undergo a further transition at 113 GPa to the orthorhombic $oC4$ structure seen in Ce and Pr at only 5 GPa and 20 GPa, respectively[3,26–28]. This would then appear to be the next structure in the general lanthanide transition sequence, but with a transition pressure that increases greatly with atomic number (from 5 GPa for Z=58 to 113 GPa for Z=60). Here we describe diffraction studies on Nd to above 300 GPa which were performed (i) to confirm that the post-$hP3$ phase has the $oF8$ structure, (ii) to determine the nature of the $oF8$ structure immediately prior to the transition to the $oC4$ phase, thereby providing information from which we might predict where the same transition will occur in Sm, and (iii) to determine whether Nd undergoes a further transition over this pressure range to the post-$oC4$ phase reported in Pr above 147 GPa[29]. We have also conducted elec-

tronic structure calculations of the $hP3$, $oF8$ and $oC4$ phases of both Nd and Sm to provide insight into the observed structural behaviour, to calculate the magnetic behaviour of Nd, and to estimate the pressure of the $oF8 \rightarrow oC4$ transition in Sm.

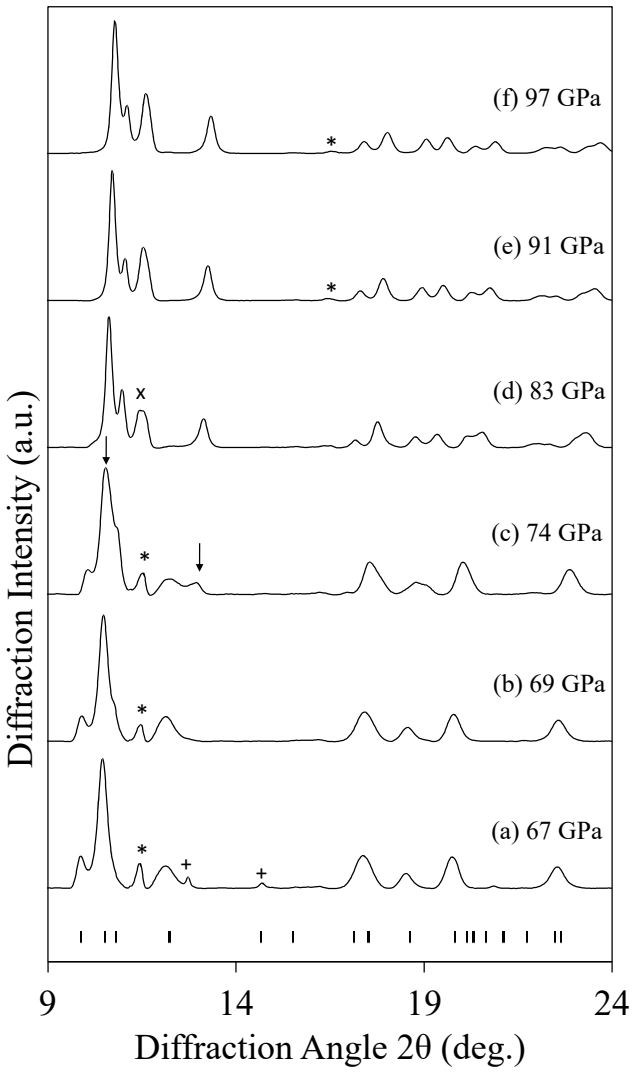

FIG. 1. Diffraction profiles collected from Nd on pressure increase to 97 GPa. The data were collected from the same sample at DLS using a wavelength $\lambda = 0.4246$ Å. Tick marks beneath profile (a) mark the calculated peak positions in the $hP3$ phase at this pressure. The peaks marked with asterisks are from the W gasket, and the peaks marked with a + are from the Cu calibrant. The two arrows in profile (c) mark the first appearance of peaks from the post-$hP3$ phase. The peak labelled with a '×' in profile (d) is a closely-spaced doublet which includes the (110) peak from the W gasket and a peak from the new phase. Single-phase patterns from the post-$hP3$ phase are seen in profiles (e) and (f).

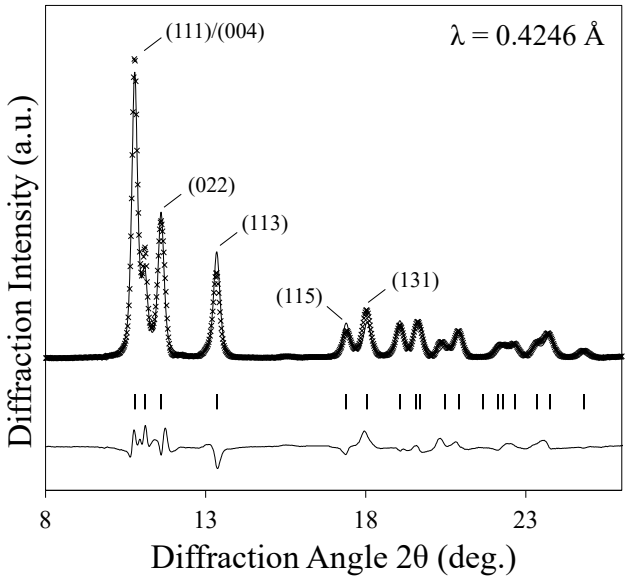

FIG. 2. Rietveld refinement of the $oF8$ structure to a diffraction profile from Nd at 97 GPa, showing the observed (crosses) and calculated (line) diffraction patterns, the calculated reflection positions, and the difference profile ($R_P = 1.8\%$, $R_{wP} = 2.5\%$, goodness of fit (GoF) = 0.46, $R(F^2) = 6.1\%$). The first six peaks of the $oF8$ phase are labelled with their Miller indices.

II. EXPERIMENTAL DETAILS

High-purity distilled samples of Nd supplied by Ulrich Schwarz at the Max-Planck-Institut für Chemische Physik fester Stoffe in Dresden were loaded into two diamond-anvil cells (DACs) in a dry argon atmosphere (<1 ppm O_2 and <1 ppm H_2O) to prevent oxidation. The DACs were equipped with diamonds with 300 μm culets, bevelled to diameters of 50 μm and 100 μm, and tungsten (W) gaskets. The samples were loaded without any pressure transmitting medium to prevent contamination. Both samples were loaded with a small (few μm) copper (Cu) sphere to act as a pressure calibrant, using the recently-published Cu equation of state of Sokolova *et al.*[30]. However, in one cell the Cu sphere was lost on closing the DAC, and the sample pressure was subsequently determined using the diamond Raman mode method[31].

Diffraction data were collected in two experiments on the high-pressure I15 beamline at the Diamond Light Source (DLS), United Kingdom, and in a further two experiments on the Extreme Conditions P02.2 beamline at the PETRA-III synchrotron in Hamburg, Germany. Further low-pressure data were obtained in 2008 on beamline 9.5HPT at the now-closed Synchrotron Radiation Source (SRS) at Daresbury Laboratory in the UK. Monochromatic x-ray beams of wavelength 0.4246Å (DLS), 0.2898Å and 0.4830Å (PETRA-III) and 0.4438Å (SRS), focused down to 20 μm × 20 μm (DLS), 0.85 μm

× 0.85 μm and 3 μm × 6 μm (PETRA-III) and 50 μm × 50 μm (SRS) were used, and the powder-diffraction data were recorded on Perkin-Elmer (PETRA-III) and Mar345 (DLS and SRS) area detectors, placed 300-400 mm from the sample. LaB_6 and CeO_2 diffraction standards were used to calibrate the exact sample-detector distances and the detector tilts in each experiment. The 2D diffraction images collected at each pressure were integrated azimuthally using Fit2D[32] and Dioptas[33] to obtain standard 1D diffraction profiles, which were then analysed using Rietveld and Le Bail profile-fitting methods[34] or by fitting to the measured d-spacings of individual diffraction peaks[35]. The sub-micron beam available at PETRA-III enabled us to map the pressure distribution in each sample at 166 GPa and the results are given in Figs. S1 and S2 in the Supplementary Information[36].

III. RESULTS AND DISCUSSION

Diffraction patterns were initially collected up to 40 GPa and the data confirmed the phase transition sequence reported previously, including the existence of the orthorhombic $oI16$ phase, previously observed between the $hR24$ and $hP3$ phases[3,37]. Evans reported the transition to $oI16$ to start at 25.8 GPa, with a transition to the $hP3$ phase above 40 GPa, in agreement with current study.

On compression above 40 GPa (see Figure 1), the $hP3$ phase was found to be stable to 71(2) GPa where a transition to the post-$hP3$ phase was observed (as illustrated in Figure 1 (c)). Above this pressure, the diffraction peaks from the $hP3$ phase decreased in intensity while those from the post-$hP3$ phase became more intense (see Figure 1 (d)). Single-phase profiles of the higher-pressure phase were seen above 90 GPa (see Figure 1 (e) and (f)), and these are strikingly similar to those obtained from the $oF8$ structure of Sm at pressures above 157 GPa[21].

Figure 2 shows a Rietveld fit of the $oF8$ structure to the background-subtracted diffraction profile obtained from Nd at 97 GPa, where the refined lattice parameters are a = 2.681(1) Å, b = 4.781(1) Å, and c = 8.783(1) Å, V/V_0=0.413(2), with atoms on the 8a site of spacgroup $Fddd$ at (0,0,0). The fit is excellent, with all of the observed diffraction peaks being accounted for.

Further compression of the sample (see Figure 3) showed that the $oF8$ phase was stable to 98(1) GPa, where the appearance of new diffraction peaks signalled a phase transition to the post-$oF8$ phase. This transition was sluggish, and single-phase profiles from the higher-pressure phases, which were very similar to those reported previously by Chesnut *et al.*[38], were obtained only above 170 GPa.

Figure 4 shows a Rietveld fit of the $oC4$ structure to the background-subtracted diffraction profile from Nd at 302 GPa, the highest pressure reached in this study. The refined lattice parameters at this pressure

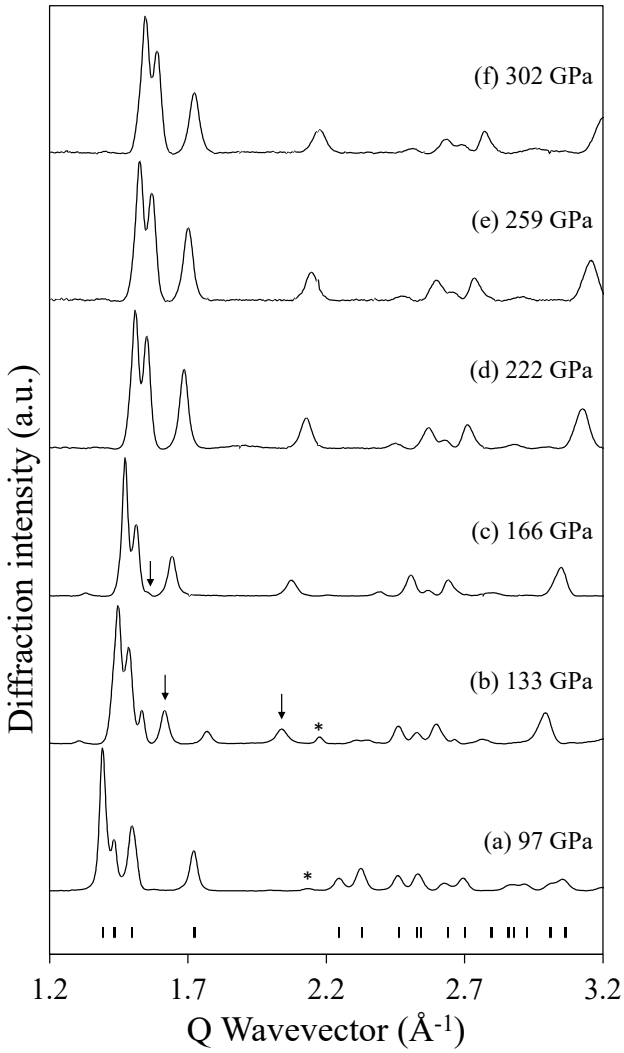

FIG. 3. Diffraction profiles collected from Nd on pressure increase to above 300 GPa. The data were collected from two samples at DLS and PETRA-III using wavelengths of λ = 0.4246 Å(DLS) and λ = 0.4830 Å(PETRA-III) and so are plotted as a function of wave vector Q so as to take into account the two different wavelengths. Tick marks beneath profile (a) mark the calculated peak positions of the $oF8$ phase. The peaks marked with the asterisks in profiles (a) and (b) are from the W gasket. The two arrows in profile (b) mark the appearance of peaks from the $oC4$ phase, and the arrow in profile (c) marks the almost complete disappearance of a peak from the remainder of the $oF8$ phase. Single-phase patterns are seen in profiles (d), (e) and (f).

are a = 2.280(1) Å, b = 4.515(1) Å, and c = 4.129(2) Å, V/V_0=0.312(6), with atoms on the 4c site of spacegroup $Cmcm$ at (0,0.114(6),0.25). The fit is again very good, with all of the observed diffraction peaks being accounted for. The misfits in peak intensities arise from the textured nature of the sample.

Nd is the only lanthanide in which the $oF8 \rightarrow oC4$

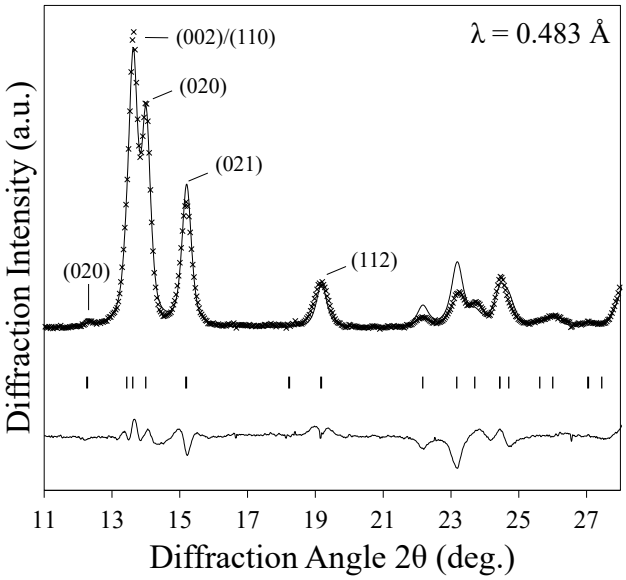

FIG. 4. Rietveld refinement of the $oC4$ structure to a diffraction profile from Nd at 302 GPa, showing the observed (crosses) and calculated (line) diffraction patterns, the calculated reflection positions, and the difference profile (R_P = 0.7%, R_{wP} = 1.1%, GoF = 0.33, $R(F^2)$ = 8.2%). The first six observable peaks of the $oC4$ phase are labelled with their Miller indices.

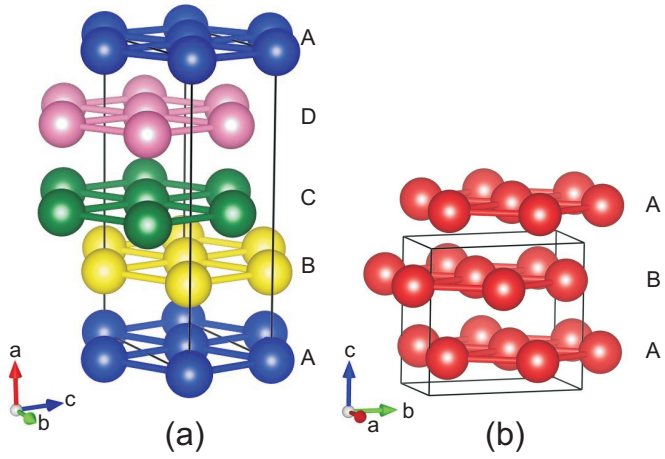

FIG. 5. The crystal structures of (a) $oF8$-Nd at 100 GPa and (b) $oC4$-Nd at 105 GPa. Both structures comprise stackings of flat, distorted-hcp atomic layers: the 4-layer stacking sequence in $oF8$ is ABCD, while $oC4$ has a 2-layer ABAB repeat. The distortion of the layers from hexagonal symmetry can be quantified by the deviation of the b/c axial ratio in $oF8$-Nd, and the b/a axial ratio in $oC4$-Nd, from the 'ideal' ortho-hexagonal value of $\sqrt{3}$=1.732.

transition has been observed to date. However, the similarity of the phase transition sequences in Nd and Sm at lower pressures suggests that the latter will also transform to the $oC4$ structure, but at pressures higher than have been reached to date (222 GPa)[21]. It is therefore of interest to determine whether the structural data obtained from the present study might enable us to predict at which pressure $oF8$-Sm will become unstable and transform to the $oC4$ structure.

The $oF8$ structure comprises a 4-layer ABCDA stacking of flat, quasi-close packed layers, the distortion of which from hexagonal symmetry can be quantified by the deviation of the b/c axial ratio from the ideal ortho-hexagonal value of $\sqrt{3}$= 1.732. The $hP3$ structure comprises a 3-layer ABC stacking of the same layers, which are exactly hexagonal in this case. The $oC4$ structure can also be described as a 2-layer stacking of heavily-distorted hcp layers with their distortion being quantified by deviations of the b/a ratio from the ideal ortho-hexagonal value of 1.732. The structures of $oF8$-Nd at 100 GPa and $oC4$-Nd at 105 GPa are shown in Figure 5, presented so as to highlight the arrangement of the quasi-hcp layers in each.

The pressure dependence of the b/c ratio in $oF8$-Nd is shown in Figure 6, along with the ideal value of $\sqrt{3}$ in the $hP3$ phase, and the b/a ratio in the $oC4$ structure. As was seen previously in Sm[21], there is a clear discontinuity in the "hexagonality" of the atomic layers from 1.732 to ∼1.78 at the $hP3 \rightarrow oF8$ transition. However, in contrast to Sm, where the b/a ratio of $oF8$-Sm increases monotonically with pressure, reaching a value of 1.82 at 222 GPa[21], the b/a ratio of $oF8$-Nd remains constant with pressure at ∼1.79 up to 100 GPa where the transition to the $oC4$ structure results in a further sharp increase in the axial ratio to ∼1.92, increasing to ∼1.98 at 120 GPa, after which the ratio is little changed by pressure up to 302 GPa. As the b/a ratio of $oF8$-Sm passes through the value of 1.79 at ∼140 GPa without undergoing a transition to the $oC4$ structure, the hexagonality of the atomic layers in the $oF8$ structure would seem to offer no insight into either the $oF8 \rightarrow oC4$ transition pressure or the transition mechanism.

The compressibility of Nd up to 302 GPa is shown in Figure 7. There are no detectable volume changes at any of the phase transitions up to the $hP3$ phase at 50 GPa, but at the $hP3 \rightarrow oF8$ and $oF8 \rightarrow oC4$ transitions there are small volume changes ($\Delta V/V_0$) of 0.4(2)% and 0.4(1)%, respectively. Despite these, the full compression curve can be fitted with a single equation of state (EoS) with little loss of accuracy.

In our recent studies of Sm[21] and Y[40], we utilised Holzapfel's APL equation of state (EoS) formalism to analyse the compressibility. This EoS has several advantages over other formalisms, and enables the compressibility to be linearised straightforwardly. Non-linear behaviour can then be interpreted as arising from deviations from "regular" compressive behaviour expected from a "normal" metal, perhaps arising from changes in the electronic structure[41].

If one fits the compression data using the second order

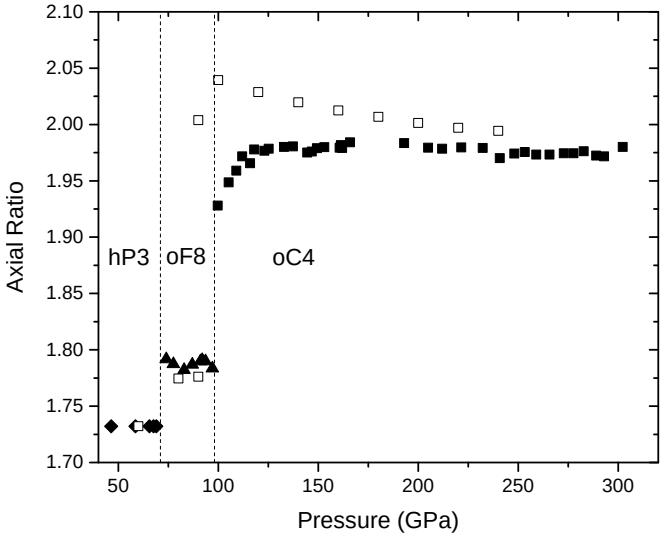

FIG. 6. The pressure dependence of the hexagonality of the atomic layers in the $hP3$, $oF8$ and $oC4$ structures of Nd, as quantified by the b/a ($hP3$ and $oC4$) and b/c ($oF8$) axial ratios - see Figure 5. Because of the extended y-scale, the error bars on the axial ratios are smaller than the symbols used to plot the points, and have therefore been omitted. The experimental data points are shown with filled symbols, while the computed values are shown using unfilled symbols.

(AP2) form of the Adapted Polynomial of order L (APL) EoS[42,43]:

$$P = 3K_0 \frac{(1-x)}{x^5} \exp(c_0(1-x))(1 + x\sum_{k=2}^{L} c_k(1-x)^{k-1}) \quad (1)$$

where K_0 is the zero pressure bulk modulus, K' is its pressure derivative, $x = (V/V_0)^{1/3}$, $c_0 = -\ln(3K_0/p_{\rm FG})$, $c_2 = (3/2)(K'-3) - c_0$, $p_{\rm FG} = a_{\rm FG}(Z/V_0)^{5/3}$ is the Fermi-gas pressure, Z is the atomic number, and $a_{\rm FG} = [(3\pi^2)/5](\hbar^2/m_e)$ =0.02337 GPa nm^5 is a constant, then the compression data can be linearised in a so-called $\eta_{\rm APL} - x$ plot:

$$\eta_{\rm APL}(x) = \ln(\frac{px^5}{p_{\rm FG}}) - \ln(1-x) \quad (2)$$

To highlight the similarities and differences in compression data of different lanthanides with respect to "ideal" behaviour, and to also highlight the systematics in phase transition pressures, it is most convenient to use an APL linearisation not with respect to x but rather with respect to the radius ratio R_{WS}/R_I[1], where R_{WS} is the pressure dependent WignerSeitz radius

$$R_{WS} = \frac{3}{4\pi}(V_{\rm atom})^{\frac{1}{3}} \quad (3)$$

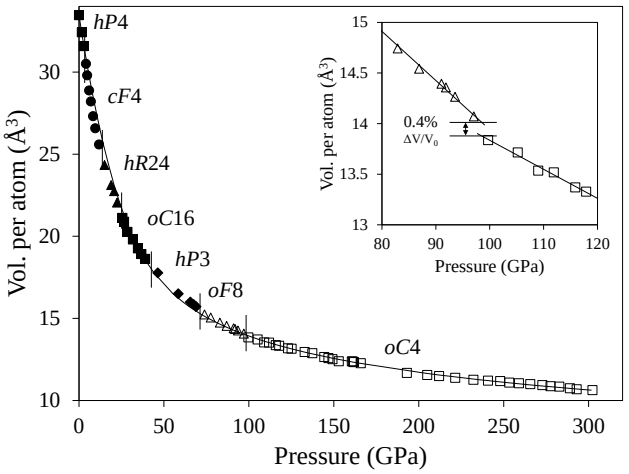

FIG. 7. The compressibility of Nd up to 302 GPa. The solid line shows the best fitting third-order APL EoS to the full compression curve. The inset shows an enlarged view of the volume near 100 GPa, illustrating the small volume discontinuity ($\Delta V/V_0$) of 0.4% and change in compressibility at the transition.

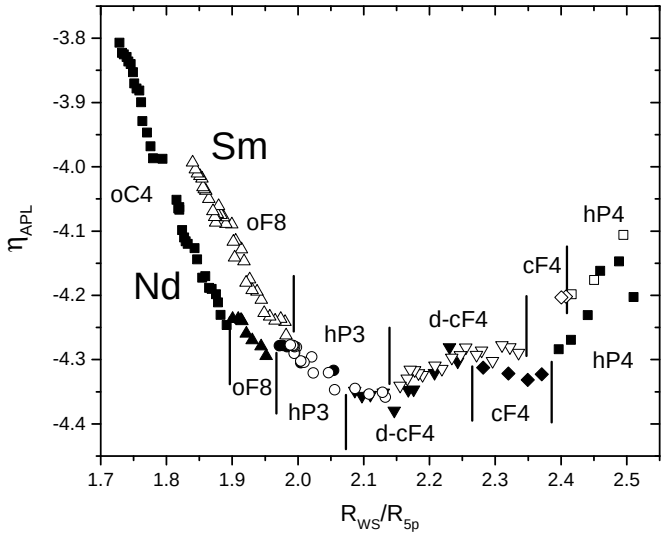

FIG. 8. Linearisation of the compression of Nd shown in the form of an η_{APL}-R_{WS}/R_{5p} plot, where R_{WS} is the Wigner-Seitz radius in angstroms and R_{5p} is the $5p$ ionic radius[39]. The data from the different phases of Nd are plotted using different symbols, and the phase boundaries are marked with vertical lines. The $hR24$ (Sm) phase, and the $hR24$ and $oI16$ phases (Nd), are labelled as 'd-$cF4$'.

and R_I is a pressure independent individual value for the ionic radius of each element[43]. The pressure dependent values of R_{WS} were determined from the measured atomic volumes, while R_I were taken to be the R_{5p} radii[44], as tabulated by Waber and Cromer[39].

Figure 8 shows the APL linearised compression data

for Nd in the form of a η_{APL} – R_{WS}/R_{5p} plot, along with the recently-published data for Sm to 222 GPa[21]. In such a plot, materials undergoing regular compression will show linear or quasi-linear behaviour, with the correct theoretical limit of $\eta(0)$=0. This is certainly not the case for Nd, the data for which exhibit significant curvature, very similar to that observed in Sm[21]. As in Sm, there is a striking change in behaviour within the $hP3$-Nd phase, such that both $oF8$-Nd and $oC4$-Nd display the linear behaviour expected of a "regular" metal, and with a gradient very similar to that exhibited by $oF8$-Sm[41].

Kruger *et al.* have previously reported[44] that constant critical radii ratios R_{WS}/R_{5p} are observed for the equilibrium values of the three transitions between the $hP2$, $hR9$, $hP4$ and $cF4$ structures of the regular trivalent lanthanides, suggesting that these transitions arise from changes in the d-band occupancy without any essential contributions from $4f$ electron bonding. At that time, the evidence suggested that the transitions to the 'special' low-symmetry structures at higher pressures, that is $hR24$, $oF8$, $oF16$ and $oC4$, did not occur at similarly critical radii, perhaps suggesting the role of $4f$ electron delocalization in these transitions[44].

Figure 8 shows the locations of all the now known phase transitions in Nd and Sm. The $oI16$ phase is seen only in Nd and, as a distorted-$cF4$ phase[3], it has been combined with the $hR24$-Nd phase in Figure 8 and labelled "d-$cF4$'.

The phase boundaries in Nd are displaced systematically to lower values of R_{WS}/R_{5p} (i.e. higher pressures) compared to those observed in Sm, with a displacement of 0.1 or less. What then stands out is the extended stability range of $oF8$-Sm, which extends down to R_{WS}/R_{5p}=1.84, whereas Nd transforms into the $oC4$ structure at R_{WS}/R_{5p}=1.90. Taking into account the offset in R_{WS}/R_{5p} between the transitions in Nd and Sm, Figure 8 suggests we would expect a transition to $oC4$-Sm at R_{WS}/R_{5p}~1.91, equivalent to a pressure of ~145 GPa.

The non-linear behaviour of Nd illustrated in Figure 8 means that its compressibility cannot be fitted by a single second-order AP2 EoS (see Figure S3). However, as was the case with Sm and Y, the compression curve of Nd *can* be fitted with the third-order AP3 EoS, as illustrated in Figure 7, which shows both the compression curve to 302 GPa, and the AP3 fit. The best-fitting parameters are K_0 = 37.2(2) GPa, K' = 1.57(2) and K'' = -0.051(2). It can be seen from the curve that the AP3 fit slightly underestimates the compressibility of the $hP4$, $cF4$ and $hR24$ phases in order to more accurately fit the higher-pressure data.

IV. ELECTRONIC STRUCTURE CALCULATIONS

To gain further insight into the behaviour of Nd at high compression, we have performed extensive DFT calculations of the $oF16$, $oF8$, $oC4$ and $hP3$ phases. Structural optimisation of bulk Nd in each phase was accomplished by using DFT calculations with the VASP[45] package, utilising the Perdew-Burke-Ernzerhof functional[46]. The k-point sampling was performed using Monkhorst-Pack meshes, ensuring a k-point density of at least 0.2Å^{-1} for all the structures and a Gaussian smearing of 0.1 eV. During the DFT structural optimization, a convergence on internal forces and stress tensor of 0.01 eV/Å was reached, and the energy cutoff was set to 500 eV. Scalar relativistic spin-orbit coupling was taken into account within the Koelling-Harmon approximation[47].

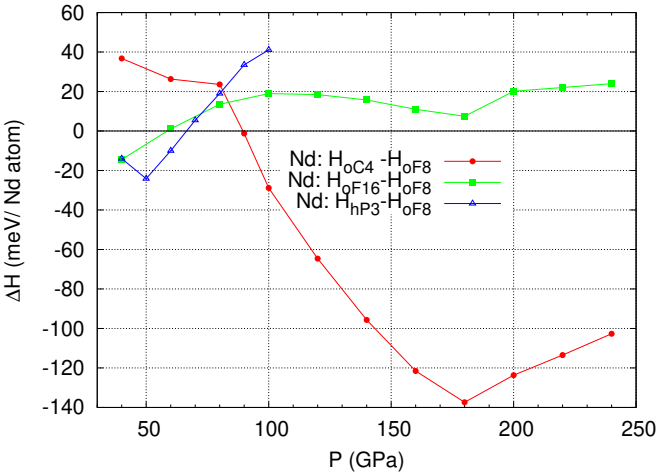

FIG. 9. The enthalpy gain of the $hP3$, $oC4$ and $oF16$ phases relative to that of the $oF8$ phase. Notice the range of pressure between 60 and 90 GPa where the $oF8$ phase appears to be most stable. The $oC4$ phase becomes the most stable at pressures above 90 GPa. $hP3$ phase is most stable below 60 GPa. The kinks on the curves correspond the loss of magnetisation.

Our zero-temperature DFT calculations for Nd reveal a series of phase transitions on compression as shown in Figure 9. Namely, by comparing the total enthalpy of the three phases examined ($hP3$, $oF8$ and $oC4$) we find that the $hP3$ phase has the lowest enthalpy up to 66 GPa, after which the $oF8$ has the lowest enthalpy to 88 GPa, with the $oC4$ phase having the lowest enthalpy above that pressure. The calculated transition pressures of 66 GPa and 88 GPa are 5-10 GPa lower than the experimentally observed transition pressures of 71(2) and 98(1) GPa seen experimentally at room temperature.

The relative enthalpy gain for the $oF8$ and $oC4$ phases shown in Figure 9 exhibits a number of kinks which can be traced back to the loss of magnetisation, as illustrated in Figure 10. The two lowest-enthalpy phases above 70 GPa, $oC4$ and $oF8$, exhibit a profoundly different magnetisation behaviour as a function of pressure: while $oC4$-Nd loses its magnetic order at 100 GPa, $oF8$-Nd does so only at 200 GPa, well outside its calculated stability range of 66-88 GPa. The loss of the magnetisation in $oC4$-Nd leads to a reduction in its atomic volume, which is clearly visible at 90 GPa in the calculated compress-

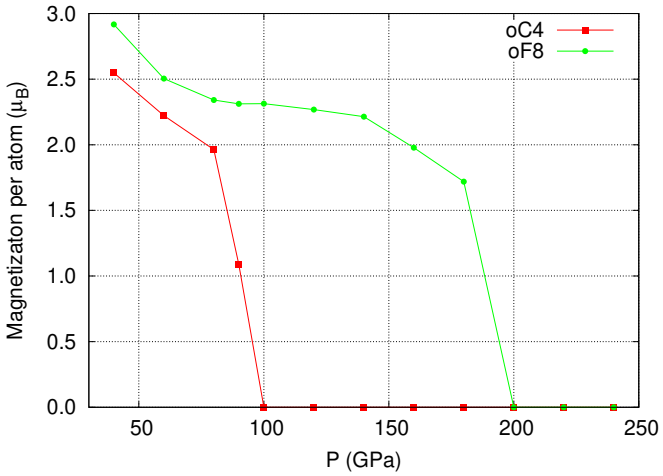

FIG. 10. The calculated magnetisation, in μ_B/atom, of $oF8$-Nd and $oC4$-Nd as a function of pressure. The magnetisation in $oC4$-Nd is greatly reduced at 90 GPa, and is zero at 100 GPa - the pressure where it is first observed experimentally. The magnetisation of $oF8$-Nd decreases rapidly only above 180 GPa, well beyond the upper pressure at which it is stable.

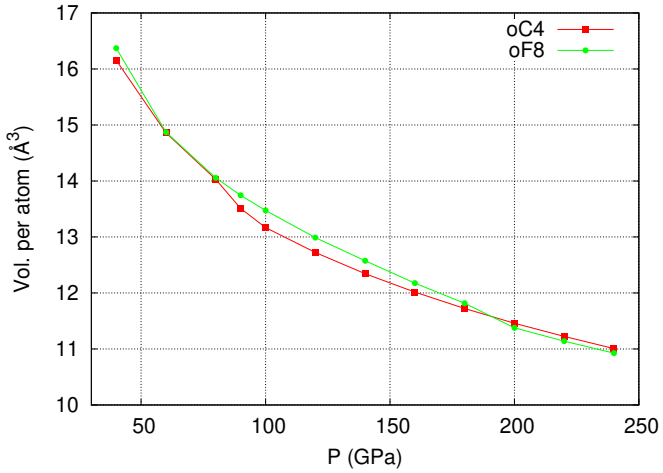

FIG. 11. The calculated volume per atom of $oF8$-Nd and $oC4$-Nd over the pressure range 40-240 GPa. The loss of magnetisation in $oC4$-Nd at 90 GPa is accompanied by a volume change ($\Delta V/V_0$) of 0.9% and a reduction in the compressibility.

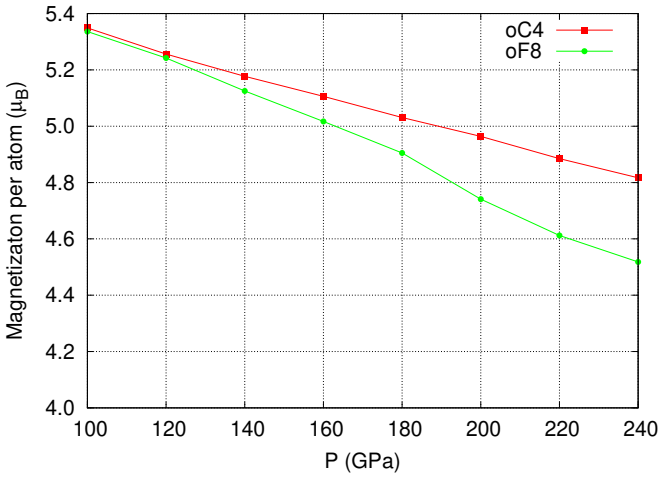

FIG. 12. The calculated magnetisation, in μ_B/atom, of the $oC4$ and $oF8$ phases of Sm over the pressure range from 100 to 240 GPa. In contrast to the behaviour seen in Nd, the magnetisation, although decreases, is non-zero in both phases at all pressures.

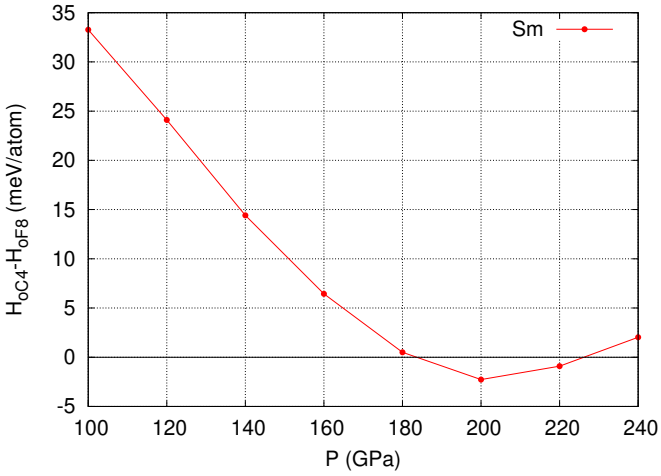

FIG. 13. The enthalpy gain of $oC4$-Sm relative to that of the $oF8$-Sm over the pressure range $100 - 240$ GPa. The $oC4$ phase is more stable over only a narrow pressure range between 185 and 225 GPa, above which the $oC4$ phase is favoured. Note the greatly reduced y-scale in comparison to Figure 9.

ibilities of the $oC4$ and $oF8$ phases shown in Figure 11, and also a sharp reduction in its enthalpy such that it becomes lower than that of the $oC4$ phase above 90 GPa. Without this loss of magnetisation, the enthalpy curves (Figure 10) suggest that $oF8$-Nd would have remained the most stable phase to much higher pressures.

The $oF8 \rightarrow oC4$ transition occurs at 98(1) GPa at 300 K, and our calculations therefore suggest that the experimentally-observed $oC4$ phase has no net magnetization. This is in agreement with the low temperature resistivity measurements of Song *et al.*[7], which showed the magnetic ordering temperature (T_0) of Nd to drop to 0 K above ∼130 GPa. The lack of a sharp drop in T_0 at 100 GPa might arise from the sluggish nature of the $oF8 \rightarrow oC4$ transition, such that the sample is mixed-phase until 170 GPa. This same argument was made by Velisavljevic *et al.* to explain the gradual decrease in resistivity they observed in Nd above 100 GPa[48].

The calculated magnetic transition and associated volume change in $oC4$-Nd is intriguing, as the volume change ($\Delta V/V_0$) of 0.9% at 100 GPa should be easily detectable by x-ray diffraction. The sluggishness of the $oF8 \rightarrow oC4$ transition on pressure increase at 300 K means that $oC4$-Nd is only a minority component of the sample

near 100 GPa. However, there are still sufficient Bragg peaks to determine its volume with high precision, as demonstrated in Figure 7, and these measurements show no evidence of any volume discontinuity after the transition to $oC4$, although there is a reduction in compressibility, as highlighted in the inset to Figure 7. This may suggest that the sample is already in the higher-density, non-magnetic state, and that the transition within the $oC4$ phase takes place at a pressure below 100 GPa. In that case, the sluggishness seen on compression suggests that the reverse $oC4 \rightarrow oF8$ transition will also take place over a large pressure range on decompression. As a result, a single-phase $oC4$-Nd sample obtained above 170 GPa on compression might be retained as single-phase $oC4$-Nd below 100 GPa on decompression. If there is a magnetic transition in $oC4$-Nd at these lower pressures, then this might be apparent from changes in the resistivity of the sample on cooling, as has been used to measure the ordering temperature in the lower-pressure $oF8$ and $hP3$ phases of Nd[7]. Simultaneous x-ray diffraction measurements would both ensure that the sample remained single-phase $oC4$-Nd, and enable the 0.9% volume change predicted to accompany the magnetic transition (Fig. 12) to be observed and measured. Further studies at both room- and low-temperature are thud required.

For comparison with our calculations on Nd, we have also made DFT calculations of the $oF8$ and $oC4$ phases of Sm, which reveal very different behaviour. $oC4$-Sm and $oF8$-Sm are very close in volume and energy at all pressures, and, crucially, while the magnetisation of $oF8$-Sm and $oC4$-Sm decreases with pressure, it does not go to zero in either phase up to 240 GPa (see Figure 12). The $oC4$ phase is calculated to have the lower enthalpy over only a small pressure range of 185-225 GPa (see Figure 13), and, even then, the enthalpy gain per atom is very small, 2 meV/atom at most (compare the y-axis scales of Figs 13 and 9). This small stability range, and the very small enthalpy gain at 0 K, probably explains why $oC4$-Sm has not been observed experimentally over this pressure range at room temperature. It is also possible, of course, that the $oF8 \rightarrow oC4$ transition in Sm takes place at a pressure higher than calculated, which is close to the highest pressure at which Sm has been studied to date (222 GPa).

In either case, it is clear that the $oF8 \rightarrow oC4$ transition pressure in Nd and Sm has little correlation with the R_{WS}/R_{5p} ratio. While we originally interpreted the different behaviour as $oF8$-Sm having a greatly extended stability range, it is perhaps more correct to see the stability range of $oF8$-Nd as greatly reduced. As said, it is the loss of magnetisation in $oC4$-Nd that results in its rapid decrease in enthalpy relative to the $oF8$ phase, and without this the transition pressure between the two phases would have been very much higher. As $oC4$-Sm is calculated to remain magnetic to at least 240 GPa, this greatly extends the stability range of the $oF8$-Sm phase.

V. CONCLUSIONS

The structure of Nd metal above 71(2) GPa is found to be face-centred orthorhombic ($oF8$) rather than monoclinic as reported previously. The same structure is observed in Am, Cm and Cf at high pressure, and also in Sm[21]. However, this structure is different to the isosymmetric $oF16$ structure observed in the heavy trivalent lanthanides Gd-Tm (except Yb)[20] and also in Y[40,49]. $oF8$-Nd is stable to 98(1)GPa, where it transforms to the $oC4$ phase, which is itself stable to 302 GPa, the highest pressure reached in this study. High-precision measurements of the compressibility of Nd reveal that it becomes less compressible after the transition to the $hP3$ phase at 43 GPa and that in the $oF8$ and $oC4$ phases its compressibility is that of a regular metal.

Electronic structure calculations of the $hP3$, $oF8$ and $oC4$ phases of Nd predict that the $hP3 \rightarrow oF8$ and $oF8 \rightarrow oC4$ transitions take place at 66 and 88 GPa, respectively, and that the latter transition results from the loss of magnetism in $oC4$-Nd which reduces both its volume and enthalpy. Comparison calculations on the $oF8$ and $oC4$ phases of Sm, in which the $oC4$ phase has not been seen experimentally at pressures up to 222 GPa at 300 K, predict that $oC4$-Sm is the more stable of the two over only a small pressure range of 185-225 GPa at 0 K, and that the enthalpy difference between the two structures is very small. The calculations predict no loss of magnetism in $oC4$-Sm to at least 240 GPa, greatly extending the stability range of the $oF8$ phase.

VI. ACKNOWLEDGEMENTS

British Crown Owned Copyright 2021/AWE. Published with permission of the Controller of Her Britannic Majesty's Stationery Office. This work was supported by Grants (Grant No. EP/R02927X/1 and No. EP/R02992X/1) from the U.K. Engineering and Physical Sciences Research Council (EPSRC) and experimental facilities made available by DESY (Hamburg, Germany), a member of the Helmholtz Association HGF, and by Diamond Light Source (DLS). We would like to thank H-P. Liermann, K. Glazyrin and R. Husband for their assistance on the ECB beamline at PETRA III, D. Daisenberger and A. Kleppe for their support on the I15 beamline at DLS, and A. Lennie for his help at the 9.5HPT beamline at SRS. S.E. Finnegan and C.V. Storm are grateful to AWE for the award of CASE studentships.

[1] B. Johansson and A. Rosengren, Physical Review B **11**, 2836 (1975).

[2] D. A. Young, *Phase Diagrams of the Elements* (University of California Press, 1991).

[3] S. R. Evans, I. Loa, L. F. Lundegaard, and M. I. McMahon, Physical Review B **80**, 134105 (2009).
[4] Y. R. Shen, R. S. Kumar, A. L. Cornelius, and M. F. Nicol, Physical Review B **75**, 064109 (2007).
[5] J. C. Duthie and D. G. Pettifor, Physical Review Letters **38**, 564 (1977).
[6] B. Johansson and A. Rosengren, Physical Review B **11**, 1367 (1975).
[7] J. Song, W. Bi, D. Haskel, and J. S. Schilling, Physical Review B **95**, 205138 (2017).
[8] J. Lim, G. Fabbris, D. Haskel, and J. S. Schilling, Physical Review B **91**, 174428 (2015).
[9] J. Lim, G. Fabbris, D. Haskel, and J. S. Schilling, Physical Review B **91**, 045116 (2015).
[10] Y. Deng and J. S. Schilling, Physical Review B **99**, 085137 (2019).
[11] G. N. Chesnut and Y. K. Vohra, Physical Review Letters **82**, 1712 (1999).
[12] G. N. Chesnut, Ph.D. thesis, The University of Alabama at Birmingham (2001).
[13] W. H. Zachariasen, Proceedings of the National Academy of Sciences **75**, 1066 (1978).
[14] D. Errandonea, R. Boehler, B. Schwager, and M. Mezouar, Physical Review B **75**, 014103 (2007).
[15] N. C. Cunningham, W. Qiu, K. M. Hope, H.-P. Liermann, and Y. K. Vohra, Physical Review B **76**, 212101 (2007).
[16] N. C. Cunningham, W. Qiu, and Y. K. Vohra, High Pressure Research **26**, 43 (2006).
[17] G. K. Samudrala, S. A. Thomas, J. M. Montgomery, and Y. K. Vohra, Journal of Physics: Condensed Matter **23**, 315701 (2011).
[18] J. M. Montgomery, G. K. Samudrala, G. M. Tsoi, and Y. K. Vohra, Journal of Physics: Condensed Matter **23**, 155701 (2011).
[19] G. K. Samudrala and Y. K. Vohra, in *Handbook on the Physics and Chemistry of Rare Earths* (Elsevier, 2013), vol. 43, pp. 275–319.
[20] M. I. McMahon, S. E. Finnegan, R. J. Husband, K. A. Munro, E. Plekhanov, N. Bonini, C. Weber, M. Hanfland, U. Schwarz, and S. G. Macleod, Physical Review B **100**, 024107 (2019).
[21] S. E. Finnegan, E. J. Pace, C. V. Storm, M. I. McMahon, S. G. MacLeod, H.-P. Liermann, and K. Glazyrin, Physical Review B **101**, 174109 (2020).
[22] J. Akella, S. T. Weir, Y. K. Vohra, H. Prokop, S. A. Catledge, and G. N. Chesnut, Journal of Physics: Condensed Matter **11**, 6515 (1999).
[23] S. Heathman, T. Le Bihan, S. Yagoubi, B. Johansson, and R. Ahuja, Physical Review B **87**, 214111 (2013).
[24] S. Heathman, R. G. Haire, T. Le Bihan, A. Lindbaum, K. Litfin, Y. Méresse, and H. Libotte, Physical Review Letters **85**, 2961 (2000).
[25] S. Heathman, R. G. Haire, T. Le Bihan, A. Lindbaum, M. Idiri, P. Normile, S. Li, R. Ahuja, B. Johansson, and G. H. Lander, Science **309**, 110 (2005).
[26] F. H. Ellinger and W. H. Zachariasen, Physical Review Letters **32**, 773 (1974), URL `https://link.aps.org/doi/10.1103/PhysRevLett.32.773`.
[27] G. S. Smith and J. Akella, Journal of Applied Physics **53**, 9212 (1982).
[28] W. A. Grosshans, Y. K. Vohra, and W. B. Holzapfel, Journal of Physics F: Metal Physics **13**, L147 (1983).
[29] N. Velisavljevic and Y. K. Vohra, High Pressure Research **24**, 295 (2004).
[30] T. S. Sokolova, P. I. Dorogokupets, A. M. Dymshits, B. S. Danilov, and K. D. Litasov, Computers & Geosciences **94**, 162 (2016).
[31] Y. Akahama and H. Kawamura, Journal of Applied Physics **100**, 43516 (2006).
[32] A. P. Hammersley and others, European Synchrotron Radiation Facility Internal Report **68**, 58 (1997).
[33] C. Prescher and V. B. Prakapenka, High Pressure Research **35**, 223 (2015).
[34] V. Petricek, M. Dusek, and L. Palatinus, Zeitschrift fur Kristallographie - Crystalline Materials **229**, 345 (2014), ISSN 21967105.
[35] T. J. B. Holland and S. A. T. Redfern, Mineralogical Magazine **61**, 65 (1997).
[36] See Supplemental Material (LINK) for additional information on the pressure distribution in the two samples, fits to the compression curve with alternative equations of states, and a summary of the 7 different structures observed in Nd on compression at room temperature, which includes Refs.[37,50].
[37] S. R. Evans, Ph.D. thesis, The University of Edinburgh (2010).
[38] G. N. Chesnut and Y. K. Vohra, Physical Review B **61**, R3768 (2000).
[39] J. T. Waber and D. T. Cromer, The Journal of Chemical Physics **42**, 4116 (1965), https://doi.org/10.1063/1.1695904, URL `https://doi.org/10.1063/1.1695904`.
[40] E. J. Pace, S. E. Finnegan, C. V. Storm, M. Stevenson, M. I. McMahon, S. G. MacLeod, E. Plekhanov, N. Bonini, and C. Weber, Physical Review B **102**, 094104 (2020), ISSN 2469-9950.
[41] W. B. Holzapfel, in *Correlations in Condensed Matter under Extreme Conditions* (Springer, 2017), pp. 91–106.
[42] W. B. Holzapfel, High Pressure Research **16**, 81 (1998).
[43] W. B. Holzapfel, Zeitschrift Fur Kristallographie **216**, 473 (2001).
[44] T. Krüger, B. Merkau, W. A. Grosshans, and W. B. Holzapfel, High Pressure Research **2**, 193 (1990).
[45] G. Kresse and D. Joubert, Phys. Rev. B **59**, 1758 (1999).
[46] J. P. Perdew, K. Burke, and M. Ernzerhof, Phys. Rev. Lett. **77**, 3865 (1996).
[47] D. D. Koelling and B. N. Harmon, Journal of Physics C: Solid State Physics **10**, 3107 (1977).
[48] N. Velisavljevic, Y. K. Vohra, and S. T. Weir, High Pressure Research **25**, 137 (2005).
[49] J. Buhot, O. Moulding, T. Muramatsu, I. Osmond, and S. Friedemann, Physical Review B **102**, 104508 (2020).
[50] J. Gonzalez-Platas, M. Alvaro, F. Nestola, and R. Angel, Journal of Applied Crystallography **49**, 1377 (2016), URL `https://doi.org/10.1107/S1600576716008050`.